

Quantum Optics with Near-Lifetime-Limited Quantum-Dot Transitions in a Nanophotonic Waveguide

Henri Thyrestrup,^{*,†} Gabija Kiršanskė,[†] Hanna Le Jeannic,[†] Tommaso Pregnolato,[†] Liang Zhai,[†] Laust Raahauge,[†] Leonardo Midolo,[†] Nir Rotenberg,[†] Alisa Javadi,[†] Rüdiger Schott,[‡] Andreas D. Wieck,[‡] Arne Ludwig,[‡] Matthias C. Löbl,[§] Immo Söllner,[§] Richard J. Warburton,[§] and Peter Lodahl^{*,†}

[†]Niels Bohr Institute, University of Copenhagen, Blegdamsvej 17, DK-2100 Copenhagen, Denmark

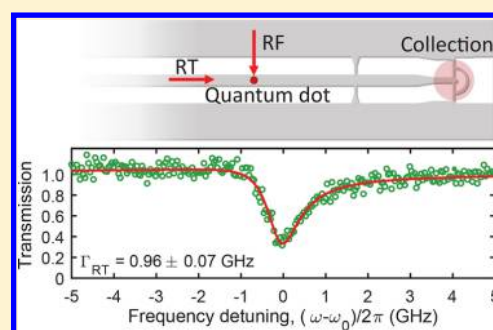
[‡]Lehrstuhl für Angewandte Festkörperphysik, Ruhr-Universität Bochum, Universitätsstrasse 150, D-44780 Bochum, Germany

[§]Department of Physics, University of Basel, Klingelbergstrasse 82, CH-4056 Basel, Switzerland

Supporting Information

ABSTRACT: Establishing a highly efficient photon-emitter interface where the intrinsic linewidth broadening is limited solely by spontaneous emission is a key step in quantum optics. It opens a pathway to coherent light–matter interaction for, e.g., the generation of highly indistinguishable photons, few-photon optical nonlinearities, and photon-emitter quantum gates. However, residual broadening mechanisms are ubiquitous and need to be combated. For solid-state emitters charge and nuclear spin noise are of importance, and the influence of photonic nanostructures on the broadening has not been clarified. We present near-lifetime-limited linewidths for quantum dots embedded in nanophotonic waveguides through a resonant transmission experiment. It is found that the scattering of single photons from the quantum dot can be obtained with an extinction of $66 \pm 4\%$, which is limited by the coupling of the quantum dot to the nanostructure rather than the linewidth broadening. This is obtained by embedding the quantum dot in an electrically contacted nanophotonic membrane. A clear pathway to obtaining even larger single-photon extinction is laid out; i.e., the approach enables a fully deterministic and coherent photon-emitter interface in the solid state that is operated at optical frequencies.

KEYWORDS: Quantum dots, resonant transmission, few-photon nonlinearity, transform-limited linewidth, nanobeam waveguide, nanophotonics



In the optical domain, the high density of optical states implies that the interaction between a single optical mode and an emitter is usually weak. As a consequence, single-photon sources, nonlinear photon–photon interactions, and photonic quantum gates are inefficient. These limitations can be overcome by placing single quantum emitters in photonic nanostructures where the routing of photons into a guided mode can be highly efficient. Additionally, the interaction between a single photon and a single quantum emitter needs to be coherent, which entails that a distinct phase relation is maintained when a single photon is scattered from the emitter; i.e., incoherent broadening mechanisms must be efficiently suppressed. Such a lifetime-limited photon-emitter interface enables indistinguishable single-photon sources^{1–5} and quantum optical nonlinearities at the single-photon level^{6–11} and may find applications in quantum many-body physics.¹² Consequently, many different solid-state quantum platforms are currently under development, each of which is based on a specific quantum emitter^{7,13–17} and with its own strengths and weaknesses. A coherent and deterministic photon-emitter interface may be a building block for complex architectures in quantum communication, toward the ultimate goal of distributed photonic quantum networks.^{18–20}

Epitaxially grown quantum dots (QDs) embedded in GaAs membranes are the basis for a particularly mature platform, as they are now routinely integrated into a variety of nanophotonic structures.²¹ By molding the photonic environment of QDs at their native nanoscale, the emitted single photons can be coupled to a guided mode with near-unity efficiency²² and made highly indistinguishable.^{3,5} The access to lifetime-limited resonance linewidths is a stricter requirement than that of indistinguishability of subsequently emitted photons since the former requires suppression of both slow drift (charge or spin noise)²³ and fast pure dephasing (phonon decoherence).^{24,25} Remarkably, this can be obtained by embedding QDs in electrically contacted bulk semiconductor structures.²⁶ However, exposed etched surfaces present in nanophotonic structures may pose a problem since they could induce charge noise in the samples. Here, we address this issue and demonstrate near-lifetime-limited photon-QD interaction in a nanophotonic waveguide. This is an essential step toward a deterministic on-chip few-photon nonlinearity, which could form the basis of, e.g.,

Received: November 28, 2017

Revised: February 6, 2018

Published: March 1, 2018

a deterministic Bell-state analyzer²⁷ and is a prerequisite for coupling multiple QDs.

Figure 1a shows the layout of the experiment. Two types of coherent measurements are performed on a QD that is efficiently

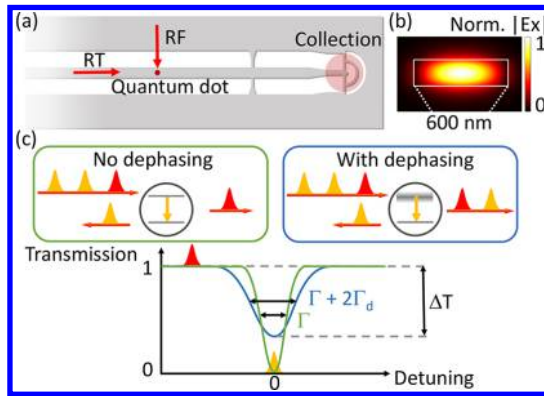


Figure 1. Resonant transmission spectroscopy on a QD in a nanobeam waveguide. (a) Sketch of the sample, which includes a QD embedded in a nanobeam waveguide that is terminated with a circular grating out-coupler. For the RF (RT) measurements, the QD is excited from free-space (the waveguide through the circular grating input-coupler), respectively; in both cases, the output signal is top-collected from the grating. (b) Calculated electric field profile of the primary mode of the nanobeam waveguide. (c) Illustration of a QD ideally coupled to the waveguide (green box), in which case all on-resonance (orange) photons are reflected while off-resonance (red) photons are transmitted, as described by a Lorentzian line shape with a width limited by the lifetime of the QD (green curve). Adding pure dephasing (blue) effectively leads to a smearing out of the excited state, thereby lowering the efficiency of the light–matter interaction and resulting in the partial transmission of on-resonant photons and a broadening of the transmission dip (blue curve). Reducing the emitter-waveguide coupling efficiency reduces the depth of the dip in both cases.

coupled to a waveguide: resonant fluorescence (RF) and resonant transmission (RT) measurements. In RF, the QD is excited at the emitter’s resonance frequency ω_0 from free-space and subsequently emits photons into the guided mode with a probability determined by the β -factor. The photons are then coupled out of the waveguide at a distant location with the help of a circular grating and are detected.

In RT, the QD is excited through the waveguide by a weak laser, and the interference between the scattered and incident photons is recorded. RT measurements on a QD were first reported in ref 28. For a QD ideally coupled to the waveguide ($\beta = 1$) and in the absence of dephasing ($\Gamma_d = 0$), the scattered and incident light interferes destructively. Thus, incident single photons resonant with the QD transition are reflected, as sketched in Figure 1c. When detuned off-resonance, the photons do not interact with the QD and are consequently transmitted. A finite pure dephasing rate Γ_d effectively smears out the energy levels and partially destroys the quantum coherence between the scattered and transmitted photons. This allows on-resonance photons to be transmitted and broadens the QD resonance, cf. illustration in Figure 1c.

The resonant scattering leads to a Lorentzian extinction dip in the transmission spectrum, whose depth depends on the effective emitter-waveguide coupling efficiency β and the pure dephasing rate of the emitter Γ_d . Here, a $\beta \neq 1$ is due to the photons that are not scattered into the waveguide mode, including the fraction of photons that are emitted into the phonon

sideband.^{29,30} The power-dependent transmission intensity on resonance is given by⁶

$$T = 1 + \frac{(\beta - 2)\beta}{(1 + 2\gamma_r)(1 + S)} \quad (1)$$

where $\gamma_r = \Gamma_d/\Gamma$ is the pure dephasing rate relative to the homogeneous linewidth Γ , and $S = n_r/n_c$ quantifies the effective saturation of the QD transition. n_r is the mean photon number within the lifetime of the emitter in the input field and n_c is the critical photon number, which can be expressed as

$$n_c = \frac{1 + 2\gamma_r}{4\beta^2} \quad (2)$$

The critical photon number represents the number of photons in the waveguide within the lifetime of the emitter resulting in an excited state population of $1/4$ for the QD. The corresponding width of the Lorentzian trough is given by

$$\Gamma_{RT} = (\Gamma + 2\Gamma_d)\sqrt{1 + S} \quad (3)$$

We note that a larger dephasing rate Γ_d causes the extinction dip to both widen and lessen, as resonant photons that would otherwise be reflected are transmitted instead. In contrast, a nonideal coupling ($\beta < 1$) only reduces the depth for a fixed decay rate. It is therefore possible to extract both β and Γ_d in the weak excitation limit ($n_r \ll n_c$) from eq 1 if the homogeneous line width Γ is known independently from lifetime measurements. The β^2 dependence of T in eq 1 makes the minimum transmission a sensitive probe of the effective β -factor whereas the dephasing rate Γ_d can be extracted from the measured linewidth. At larger incident powers the QD transition is power-broadened, as seen from eq 3, and results in a decrease of the transmission extinction.

In the following experiment the waveguide sample featured weak reflections from the termination ends, meaning that weak cavity resonances were modulating the spectral response of the system. Consequently, the transmission response has a Fano spectral character,^{6,31,32} which slightly modifies the Lorentzian profile described by eq 3. See the Supporting Information for detailed expressions for the Fano resonances that were used to model the experimental data.

The experiment is conducted on a single QD located near the center of a 600 nm wide and 175 nm thick planar GaAs nanobeam waveguide. The width was chosen to maintain a relatively large separation between the QD and nearby interfaces while still supporting a well-confined mode (see Figure 1b) with a large β -factor above 0.5. The waveguide supports three guided modes, and the higher-order modes can largely be filtered out via photonic elements on the chip (see the Supporting Information). The studied QD is located approximately 15 μm away from the collection grating, which is a second-order circular Bragg grating optimized for a wavelength of 920 nm,³³ cf. Figure 1a for a schematic with a full SEM image of the sample shown in the Supporting Information. The QD layer with a density of around 1 μm^{-2} is embedded in a p–i–n diode (see ref 5 for details) and held at a temperature of 1.7 K in order to stabilize the local charge environment and to suppress phonon broadening.^{25,29,30} Charge stabilization is essential in order to achieve narrow optical linewidths.³⁴ We consider a bright neutral exciton line X^0 of the QD with an emission wavelength of 920.86 nm at 0.2 V, cf. Figure 2a with other charge states being visible at longer wavelengths. The external bias enables tuning of the QD transition energy. The decay rate of the QD is measured by

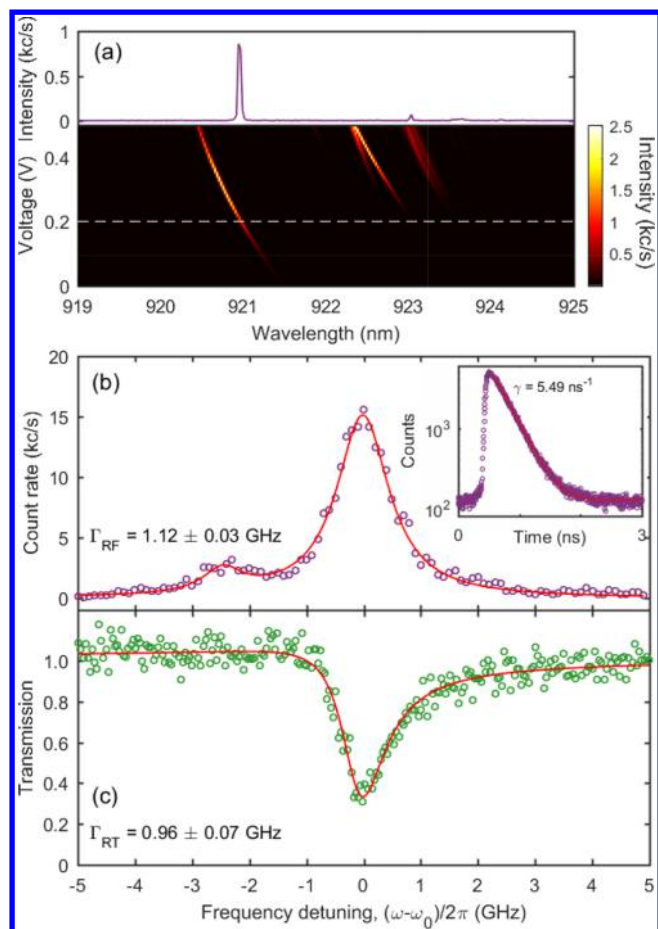


Figure 2. Photoluminescence spectroscopy on a single QD. (a) Voltage-dependent photoluminescence map (bottom panel) of the QD under above-band excitation. Full spectrum of the QD recorded at $V = 0.2$ V is shown in the top panel. Linewidth measurement from the resonance fluorescence (b) and the resonant transmission (c) configuration for the X^0 QD transition. The solid red curves represent a Lorentzian fit to the data and the Fano resonance model (cf. the Supporting Information for the detailed expression), respectively. A nearby residual peak from the same QD is modeled with a Lorentzian function as well, and is excluded from the analysis. Inset in part b: measured decay curve of the QD. The red line is the fit to a single-exponential model. The measurements were done at a sample temperature of $T = 1.7$ K.

time-correlated single photon counting on an avalanche photodiode (APD) with a response time of 50 ps where the QD is excited by a picosecond-pulsed laser tuned to the p-shell at 905.8 nm. Excitation in the p-shell prevents the excitation of free carriers, which could shield the QD from the applied field and thus potentially modify the decay rate. The measured decay curve is shown in the inset in Figure 2 and is fitted with a single exponential decay convoluted with the measured instrument response function (IRF) of the APD. The extracted decay rate is $\gamma = 5.49 \pm 0.02$ ns $^{-1}$ corresponding to a natural linewidth of $\Gamma = \gamma/2\pi = 0.87 \pm 0.003$ GHz and a lifetime of $\tau = 1/\gamma = 182$ ps. For comparison the decay rate recorded on QDs in an unstructured part of the sample is around $\gamma = 3.5$ ns $^{-1}$. This corresponds to a Purcell factor of 1.6 in the nanobeam waveguide, which is consistent with simulations for a QD located within 20 nm from the waveguide center (see the Supporting Information).

The large decay rate (short lifetime) of the QDs found both in bulk and in nano structures for the present wafer is attributed to a large QD oscillator strength.²¹ To exclude nonradiative

processes, a lower estimate of the internal quantum efficiency of the QDs was determined from measurements on two QDs on the same chip embedded in photonic-crystal waveguides, where the coupling to the waveguide strongly modifies the radiative decay rate. Here, we observed an inhibited decay rate of $\gamma_i = 1.2$ ns $^{-1}$ for a QD spectrally located inside the photonic band gap region. For comparison a greatly enhanced decay rate of up to $\gamma_e = 13.5$ ns $^{-1}$ was observed for a QD coupled to the photonic-crystal waveguide. A lower-bound estimate assumes that the inhibited rate γ_i is dominated by nonradiative processes, and we can extract an internal quantum efficiency of $\eta_{QE} \geq (\gamma_e - \gamma_i)/\gamma_e \approx 92\%$; i.e., it can be excluded that the short lifetimes originate from nonradiative recombination.

The RF spectrum is presented in Figure 2b. It was measured by scanning the frequency of a narrow-band continuously tunable diode laser (Topical CTL with <10 kHz bandwidth) from the top across the QD resonance at a fixed bias voltage of $V = 0.2$ V. The incident laser and collection are copolarized transversely to the waveguide mode. The spatial separation between the QD and the collection grating is sufficient to achieve an RF signal that is more than 200 times larger than the background laser. The line shape is well-modeled by a Lorentzian with a linewidth of $\Gamma_{RF} = 1.12 \pm 0.03$ GHz. The RF experiment was conducted at an excitation intensity of $S = 0.13$ of the saturation level, meaning that power broadening amounts to a linewidth increase of 6%. The Lorentzian line shape is evidence that the additional broadening is dominated by pure dephasing, and we estimate a pure dephasing rate of $\Gamma_d = 0.14\Gamma$. The observed nearly transform-limited linewidth shows that electrical gating of planar nanophotonic structures may overcome residual broadening due to charge noise.³⁵

For the RT measurements the laser is injected into the waveguide through an input circular grating coupler (see the Supporting Information for an electron microscope image) and then mode-filtered through a photonic-crystal waveguide followed by a single mode section to predominantly inject light into one waveguide mode. The RT spectrum on the same QD at a low excitation power of $S = 0.02$ is presented in Figure 2c. Here, the laser frequency is fixed at $\omega/2\pi = 325.457$ THz while the QD transition frequency $\omega_0/2\pi$ is tuned by the voltage over the p-i-n diode. A coarse frequency-voltage scan is used to calibrate the local frequency axis. We observe a narrow extinction of the resonant transmission with a linewidth of $\Gamma_{RT} = 0.96 \pm 0.07$ GHz, which is only broadened by 10% relative to the natural linewidth. The near-transform-limited linewidth implies that a record-high extinction of $\Delta T = 0.66 \pm 0.04$ is obtained, which is more than 1.5 times larger than previously reported for solid-state emitters integrated into nanophotonic waveguides.^{6,10,15,17} The extinction quantifies the strength of coherent interaction between a single photon and the QD and is therefore an essential figure-of-merit for quantum-information processing.²¹

The transmission spectrum in Figure 2c is modeled with the full spectral model⁶ that accounts for the effective β -factor, pure dephasing Γ_d , and coupling to Fabry-Pérot modes in the waveguide arising from residual reflections from the termination of the waveguide structure. This coupling leads to an extra phase shift and results in the asymmetric Fano-like line shape observed in Figure 2c. We extract $\beta = 0.51 \pm 0.04$ and a pure dephasing rate of $\Gamma_d = (0.06 \pm 0.04)\Gamma$; i.e., the transmission response is nearly transform-limited. For comparison the calculated pure dephasing rate is $\Gamma_d \approx 0.01\Gamma$ based on the contributions from phonons,²⁵ which is consistent with the

experimental results. We note that the 600 nm wide nanobeam supports three guided modes at the operation wavelength of 920 nm, and the extracted β is therefore to be considered as an effective coupling efficiency; i.e., the coupling to the dominating mode can be even higher.

The analysis reveals that the linewidth recorded from the RF data ($\Gamma_{\text{RF}} = 1.12 \pm 0.03$ GHz) is slightly larger than the value obtained from the RT measurement ($\Gamma_{\text{RT}} = 0.96 \pm 0.07$ GHz).

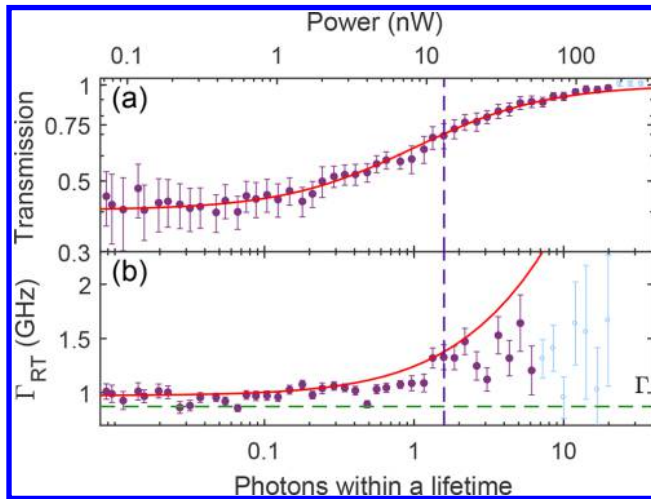


Figure 3. Saturation behavior of the resonant transmission. The transmission dip (a) and the QD linewidth (b) as a function of power at $T = 1.7$ K. The transition linewidth broadens, and the transmission extinction decreases as the emission intensity of the neutral exciton transition saturates at a characteristic input power of 13.1 nW corresponding to the fact that on average ~ 1.6 photons interact with the QD within its radiative lifetime. When the emitter is saturated, the transmission is dominated by the resonant laser and reaches the steady value of one. The homogeneous linewidth $\Gamma = 0.87$ GHz is shown as a dashed green line. The red lines are consistent model fits to the purple data points while the blue data points are omitted in the fit since the extracted values are influenced by the neighboring transition that is apparent in the data of Figure 2 and that influences the analysis at elevated pump power.

The two experiments are conducted with different experimental conditions: in the former case 15.7 nW (corresponding to 13.5 photons/lifetime) of laser power is directed to the waveguide while in the latter only 26 pW of optical power travels through the waveguide (see the Supporting Information for the detailed description). It is therefore plausible that the higher excitation intensity applied in the RF experiment may introduce a slight inhomogeneous broadening, e.g., due to light-induced activation of charge defect states introducing spectral diffusion.^{26,36} Excitingly such broadening seems to be absent in the RT experiment, where the only remaining decoherence mechanism is pure dephasing, which broadens the zero-phonon line and can potentially be suppressed at low temperatures by phonon engineering.²⁵ Note that the phonon sidebands effectively rescale the β -factor, and may be improved by enhancing the radiative decay rate through, e.g., Purcell enhancement.²¹ Consequently our work shows that the planar nanophotonic platform grants access to all required tools for constructing a fully deterministic and coherent photon-emitter interface ($\beta \simeq 1$, $\Gamma_{\text{d}} \simeq 0$) at optical frequencies.

In order to show the nonlinear interaction with the QD, power-dependent RT measurements were carried out. For each incident power a transmission spectrum similar to Figure 2c is recorded, and the extracted transmission minimum and line width are presented in Figure 3. We note that the neighboring peak in Figure 2b influences the analysis of the linewidth at higher powers, which induces fluctuations in the data in Figure 3. The experimental data are well-explained by the theory for power broadening: as the excitation power increases, the coherence of the scattered light is reduced, and the transmission converges toward unity (cf. Figure 3a). Correspondingly, the line width broadens, cf. Figure 3b. The description of the modeling of the data is given in the Supporting Information. The characteristic input power determining the saturation of the coupled QD corresponds to the fact that on average ~ 1.6 photons in the waveguide interact with the QD per emitter lifetime.

Finally, the robustness of the observed behavior to temperature is mapped out in detail. Figure 4 shows RT measurements at a low power of $P = 0.7$ nW and as a function of temperature.

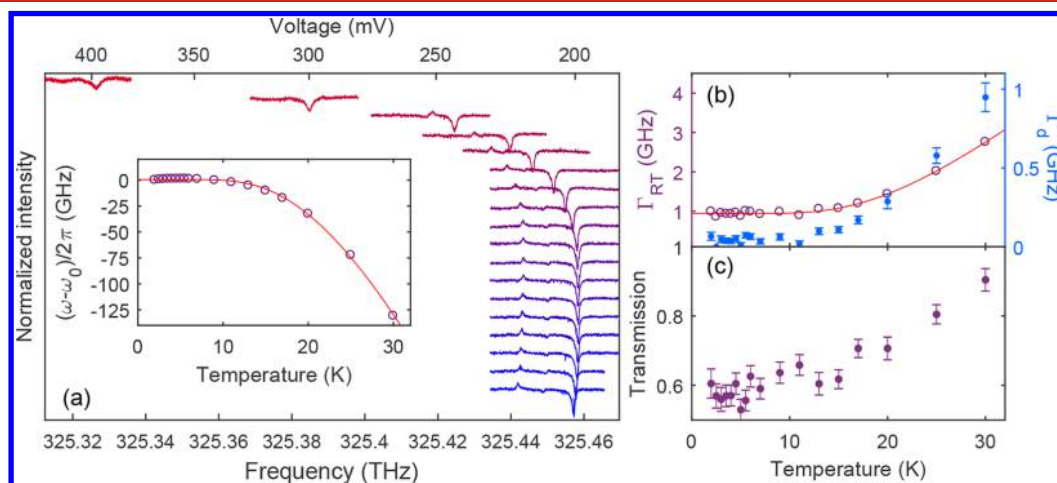


Figure 4. Temperature-dependent resonant transmission. (a) Transmission spectra recorded at 0.68 nW and at a temperature varied from 1.97 to 30 K (curves from bottom to top). The shallow dip and narrow peak observed at the low-energy side of the main feature are attributed to the resonance of another transition and another QD, respectively. The QD resonance red shifts with temperature (see the inset); thus, the voltage needed to map out the resonance is increased. The red line in the inset is a model fit to the band edge shift (see the Supporting Information). Linewidth and corresponding dephasing rate (b) and minimum (c) of the transmission resonance as a function of temperature. The red line is a guide to the eye, which illustrates the variation of the linewidth. This data set has been taken in a nonideal polarization, where multiple waveguide modes were collected with a different β -factor; thus, the transmission extinction for low temperature slightly differs from that observed in Figures 2 and 3.

The spectra are acquired by keeping the resonant laser fixed and scanning the voltages across the p–i–n diode. We find a nonlinear temperature dependence of the central position of the resonance (see the inset of Figure 4a) which is explained by the temperature dependence of the band edge of the semiconductor material. From the data series we can extract the temperature dependence of the decoherence processes. Figure 4b shows the recorded temperature dependence of the linewidth and the corresponding pure dephasing rate obtained by modeling the transmission spectra. The temperature dependence of the transmission extinction is shown in Figure 4c. Up to about 10 K, the linewidth remains nearly transform-limited, and the pure dephasing rate is therefore small. The linewidth broadens significantly at higher temperatures, which reflects the crossover between different temperature regimes in the pure dephasing rate, as predicted by theory.²⁵

We have demonstrated that highly efficient and coherent quantum light–matter interaction can be obtained in nanoscale planar waveguides, by using electrically contacted GaAs nanophotonic structures with embedded InAs QDs. In particular, we present lifetime-limited linewidth measurements of QDs as recorded in a resonance transmission experiment. The coherent and efficient coupling manifests itself in a large scattering extinction at the single-photon level of up to $\Delta T = 0.66$, which is more than 1.5 times larger than what has been previously reported.¹⁰ Future work will focus on increasing the β -factor even further, which can be straightforwardly done by decreasing the waveguide width in order to be in the single-mode regime while the potential influence of charge noise should still be eliminated. Consequently, a clear pathway to a high-cooperativity photon-emitter interface is laid out, which may enable photonic quantum gates implemented on a fully solid-state platform.³⁷ Furthermore, the exploitation of coherent nonlinear quantum optics and collective effects¹¹ provides an interesting future direction.

■ ASSOCIATED CONTENT

📄 Supporting Information

The Supporting Information is available free of charge on the ACS Publications website at DOI: 10.1021/acs.nanolett.7b05016.

Additional calculations and figures including COMSOL images, coupling efficiency and emission enhancement as a function of emitter displacement, and electron microscope image of the entire nanophotonic device (PDF)

■ AUTHOR INFORMATION

Corresponding Authors

*E-mail: henri.nielsen@nbi.ku.dk.

*E-mail: lodahl@nbi.ku.dk. Phone: +4535325306.

ORCID

Henri Thyrrestrup: 0000-0001-8922-4462

Notes

The authors declare no competing financial interest.

■ ACKNOWLEDGMENTS

We gratefully acknowledge financial support from the European Research Council (ERC Advanced Grant “SCALE”), Innovation Fund Denmark (Quantum Innovation Center “Qubiz”), and the Danish Council for Independent Research. R.S., A.D.W., and A.L. acknowledge support within the DFG SFB ICRC-TRR 160 Z1 project and BMBF-Q.com-H 16KIS0109. M.C.L.,

I.S., and R.J.W. acknowledge financial support from NCCR QSIT and from SNF Project 200020_175748.

■ REFERENCES

- (1) Santori, C.; Fattal, D.; Vučković, J.; Solomon, G. S.; Yamamoto, Y. *Nature* **2002**, *419*, 594–597.
- (2) He, Y.-M.; He, Y.; Wei, Y.-J.; Wu, D.; Atatüre, M.; Schneider, C.; Höfling, S.; Kamp, M.; Lu, C.-Y.; Pan, J.-W. *Nat. Nanotechnol.* **2013**, *8*, 213–7.
- (3) Ding, X.; He, Y.; Duan, Z.-C.; Gregersen, N.; Chen, M.-C.; Unsleber, S.; Maier, S.; Schneider, C.; Kamp, M.; Höfling, S.; Lu, C.-Y.; Pan, J.-W. *Phys. Rev. Lett.* **2016**, *116*, 020401.
- (4) Senellart, P.; Solomon, G.; White, A. *Nat. Nanotechnol.* **2017**, *12*, 1026–1039.
- (5) Kiršanskė, G.; et al. *Phys. Rev. B: Condens. Matter Mater. Phys.* **2017**, *96*, 165306.
- (6) Javadi, A.; Söllner, I.; Arcari, M.; Lindskov Hansen, S.; Midolo, L.; Mahmoodian, S.; Kiršanskė, G.; Pregolato, T.; Lee, E. H.; Song, J. D.; Stobbe, S.; Lodahl, P. *Nat. Commun.* **2015**, *6*, 8655.
- (7) Maser, A.; Gmeiner, B.; Utikal, T.; Götzinger, S.; Sandoghdar, V. *Nat. Photonics* **2016**, *10*, 450–453.
- (8) Snijders, H.; Frey, J. A.; Norman, J.; Bakker, M. P.; Langman, E. C.; Gossard, A.; Bowers, J. E.; van Exter, M. P.; Bouwmeester, D.; Löffler, W. *Nat. Commun.* **2016**, *7*, 12578.
- (9) De Santis, L.; Antón, C.; Reznichenko, B.; Somaschi, N.; Coppola, G.; Senellart, J.; Gómez, C.; Lemaitre, A.; Sagnes, I.; White, A. G.; Lanco, L.; Auffèves, A.; Senellart, P. *Nat. Nanotechnol.* **2017**, *12*, 663–667.
- (10) Hallett, D.; Foster, A. P.; Hurst, D. L.; Royall, B.; Kok, P.; Clarke, E.; Itskevich, I. E.; Fox, A. M.; Skolnick, M. S.; Wilson, L. R. **2017**, arXiv:1711.00682. *arXiv.org e-Print archive*. <https://arxiv.org/abs/1711.00682>.
- (11) Chang, D. E.; Vuletić, V.; Lukin, M. D. *Nat. Photonics* **2014**, *8*, 685–694.
- (12) Suter, D.; Álvarez, G. A. *Rev. Mod. Phys.* **2016**, *88*, 041001.
- (13) Birnbaum, K. M.; Boca, A.; Miller, R.; Boozer, A. D.; Northup, T. E.; Kimble, H. J. *Nature* **2005**, *436*, 87–90.
- (14) Sipahigil, A.; et al. *Science* **2016**, *354*, 847–850.
- (15) Bhaskar, M. K.; Sukachev, D. D.; Sipahigil, A.; Evans, R. E.; Burek, M. J.; Nguyen, C. T.; Rogers, L. J.; Siyushev, P.; Metsch, M. H.; Park, H.; Jelezko, F.; Lončar, M.; Lukin, M. D. *Phys. Rev. Lett.* **2017**, *118*, 223603.
- (16) Javadi, A. et al. **2017**, arXiv:1709.06369. *arXiv.org e-Print archive*. <https://arxiv.org/abs/1709.06369>.
- (17) Türschmann, P.; Rotenberg, N.; Renger, J.; Harder, I.; Lohse, O.; Utikal, T.; Götzinger, S.; Sandoghdar, V. *Nano Lett.* **2017**, *17*, 4941–4945.
- (18) Kimble, H. J. *Nature* **2008**, *453*, 1023–1030.
- (19) Ritter, S.; Nölleke, C.; Hahn, C.; Reiserer, A.; Neuzner, A.; Uphoff, M.; Mücke, M.; Figueroa, E.; Bochmann, J.; Rempe, G. *Nature* **2012**, *484*, 195–200.
- (20) Lodahl, P. *Quantum Sci. Technol.* **2018**, *3*, 013001.
- (21) Lodahl, P.; Mahmoodian, S.; Stobbe, S. *Rev. Mod. Phys.* **2015**, *87*, 347–400.
- (22) Arcari, M.; Söllner, I.; Javadi, A.; Lindskov Hansen, S.; Mahmoodian, S.; Liu, J.; Thyrrestrup, H.; Lee, E. H.; Song, J. D.; Stobbe, S.; Lodahl, P. *Phys. Rev. Lett.* **2014**, *113*, 093603.
- (23) Kuhlmann, A. V.; Houel, J.; Ludwig, A.; Greuter, L.; Reuter, D.; Wieck, A. D.; Poggio, M.; Warburton, R. J. *Nat. Phys.* **2013**, *9*, 570–575.
- (24) Thoma, A.; Schnauber, P.; Gschrey, M.; Seifried, M.; Wolters, J.; Schulze, J.-H.; Strittmatter, A.; Rodt, S.; Carmele, A.; Knorr, A.; Heindel, T.; Reitzenstein, S. *Phys. Rev. Lett.* **2016**, *116*, 033601.
- (25) Tighineanu, P.; Dreeßen, C. L.; Flindt, C.; Lodahl, P.; Sørensen, A. S. **2017**, arXiv:1702.04812. *arXiv.org e-Print archive*. <https://arxiv.org/abs/1702.04812>.
- (26) Kuhlmann, A. V.; Prechtel, J. H.; Houel, J.; Ludwig, A.; Reuter, D.; Wieck, A. D.; Warburton, R. J. *Nat. Commun.* **2015**, *6*, 8204.

- (27) Ralph, T. C.; Söllner, I.; Mahmoodian, S.; White, A. G.; Lodahl, P. *Phys. Rev. Lett.* **2015**, *114*, 173603.
- (28) Högele, A.; Seidl, S.; Kroner, M.; Karrai, K.; Warburton, R. J.; Gerardot, B. D.; Petroff, P. M. *Phys. Rev. Lett.* **2004**, *93*, 217401.
- (29) Besombes, L.; Kheng, K.; Marsal, L.; Mariette, H. *Phys. Rev. B: Condens. Matter Mater. Phys.* **2001**, *63*, 155307.
- (30) Favero, I.; Cassabois, G.; Ferreira, R.; Darson, D.; Voisin, C.; Tignon, J.; Delalande, C.; Bastard, G.; Roussignol, P.; Gérard, J.-M. *Phys. Rev. B: Condens. Matter Mater. Phys.* **2003**, *68*, 233301.
- (31) Shen, J. T.; Fan, S. *Opt. Lett.* **2005**, *30*, 2001.
- (32) Auffèves-Garnier, A.; Simon, C.; Gérard, J.-M.; Poizat, J.-P. *Phys. Rev. A: At, Mol, Opt. Phys.* **2007**, *75*, 053823.
- (33) Faraon, A.; Fushman, I.; Englund, D.; Stoltz, N.; Petroff, P.; Vučković, J. *Opt. Express* **2008**, *16*, 12154–12162.
- (34) Löbl, M. C.; Söllner, I.; Javadi, A.; Pregnolato, T.; Schott, R.; Midolo, L.; Kuhlmann, A. V.; Stobbe, S.; Wieck, A. D.; Lodahl, P.; Ludwig, A.; Warburton, R. J. *Phys. Rev. B: Condens. Matter Mater. Phys.* **2017**, *96*, 165440.
- (35) Liu, J.; Konthasinghe, K.; Davanco, M.; Lawall, J.; Anant, V.; Verma, V.; Mirin, R.; Nam, S. W.; Song, J. D.; Ma, B.; Chen, Z. S.; Ni, H. Q.; Niu, Z. C.; Srinivasan, K. 2017, arXiv:1710.09667. *arXiv.org e-Print archive*. <https://arxiv.org/abs/1710.09667>.
- (36) Kurzmann, A.; Ludwig, A.; Wieck, A. D.; Lorke, A.; Geller, M. *Appl. Phys. Lett.* **2016**, *108*, 263108.
- (37) Reiserer, A.; Rempe, G. *Rev. Mod. Phys.* **2015**, *87*, 1379–1418.